

Supporting Information

Highly Biocompatible Chlorin e6-Poly(dopamine) Core-Shell

Nanoparticle for Enhanced Cancer Phototherapy

Shilin Chen,¹ Yihang Jiang,¹ Miaozaung Fan,¹ Xinmeng Zhang,¹ Ying Zhang,¹ Ting Chen,² Chengbin Yang,¹ Wing-Cheung Law,^{2*} Zhou Rui Xu,^{1*} Gaixia Xu^{1*}

1. Guangdong Key Laboratory for Biomedical Measurements and Ultrasound Imaging, School of Biomedical Engineering, Health Science Center, Shenzhen University, Shenzhen 518060, China
2. Department of Industrial and Systems Engineering, The Hong Kong Polytechnic University, Hong Kong

Table of Contents

- Fig. S1. The colloidal stability of CBP NPs under different pH conditions.
- Fig. S2. The absorption spectra of ABDA after photodecomposition.
- Fig. S3. The photothermal response of CBP NPs.
- Fig. S4. The Ce6 release profiles of CBP NPs at different conditions.
- Fig. S5. The hydrodynamic size of CBP NPs before and after the light irradiation.
- Fig. S6. Confocal fluorescence microscope images of cells uptake.
- Fig. S7. Hemolysis rate of CBP NPs
- Fig. S8. Evaluation of intracellular ROS production before and after light irradiation.
- Fig. S9. Bright field photograph of live and dead staining of cells.
- Fig. S10. The *in vitro* phototherapeutic effect of CBP NPs under different conditions.
- Fig. S11. Photographs of H&E and TUNEL staining imaging of two extra groups.
- Fig. S12. Average body weight of four groups of mice.
- Fig. S13. Main organ coefficients of four groups of mice.

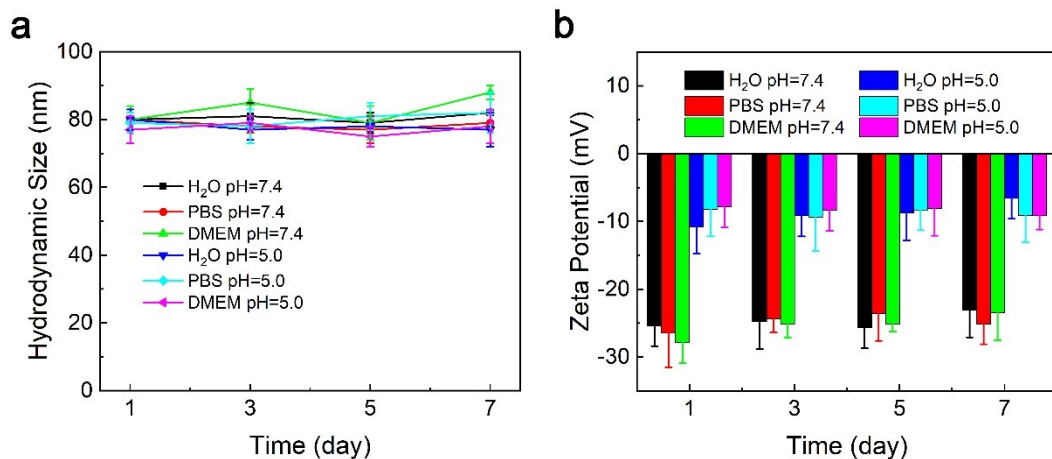


Fig. S1. The colloidal stability of CBP NPs under different pH conditions. (a) The hydrodynamic size and (b) zeta potential of CBP NPs.

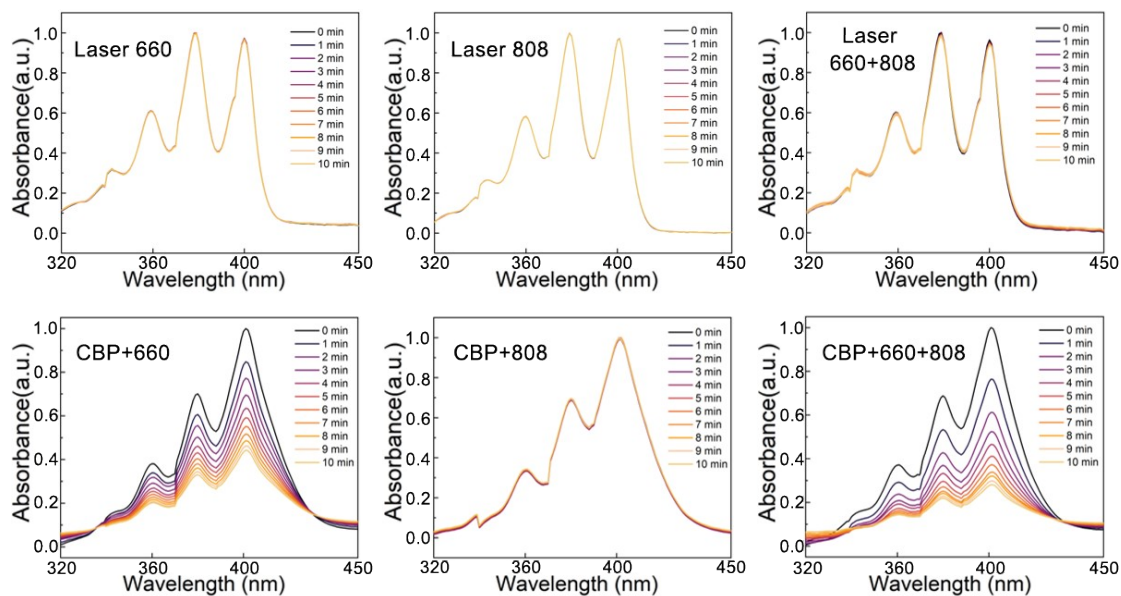


Fig. S2. Normalized absorbance of ABDA after photodecomposition by ROS generation of six groups (three groups of 660 nm, 808nm, or dual-mode laser alone and three groups of CBP NPs combined with 660 nm, 808nm, or dual-mode laser).

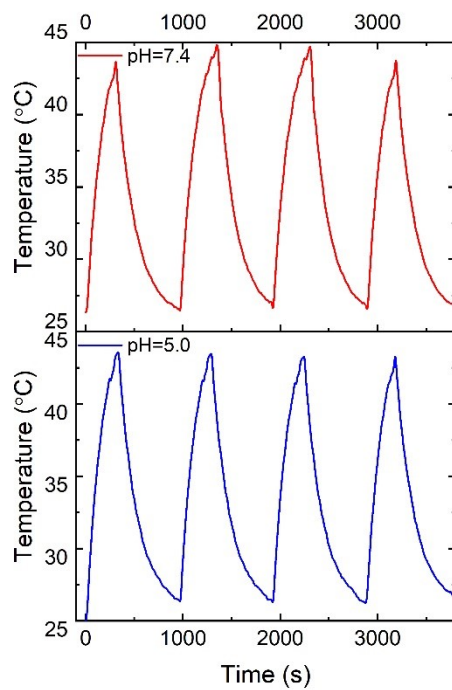


Fig. S3. The photothermal response of CBP NPs in neutral and weakly acidic conditions.

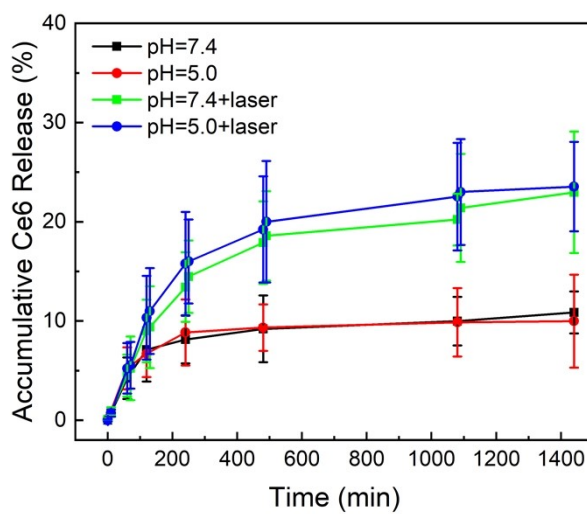


Fig. S4. The Ce6 release profiles of CBP NPs at different conditions.

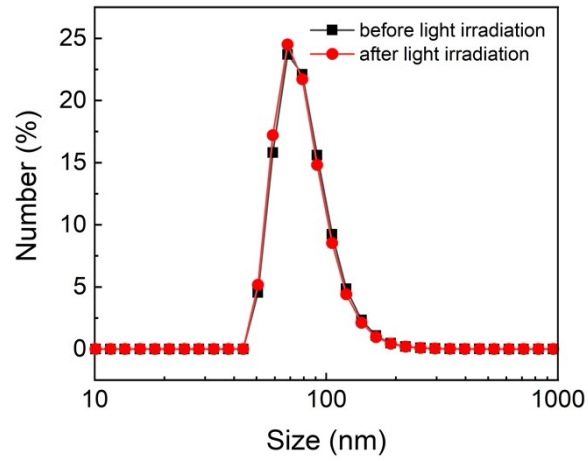


Fig. S5. The hydrodynamic size of CBP NPs in PBS buffer before and after the light irradiation of 30 minutes.

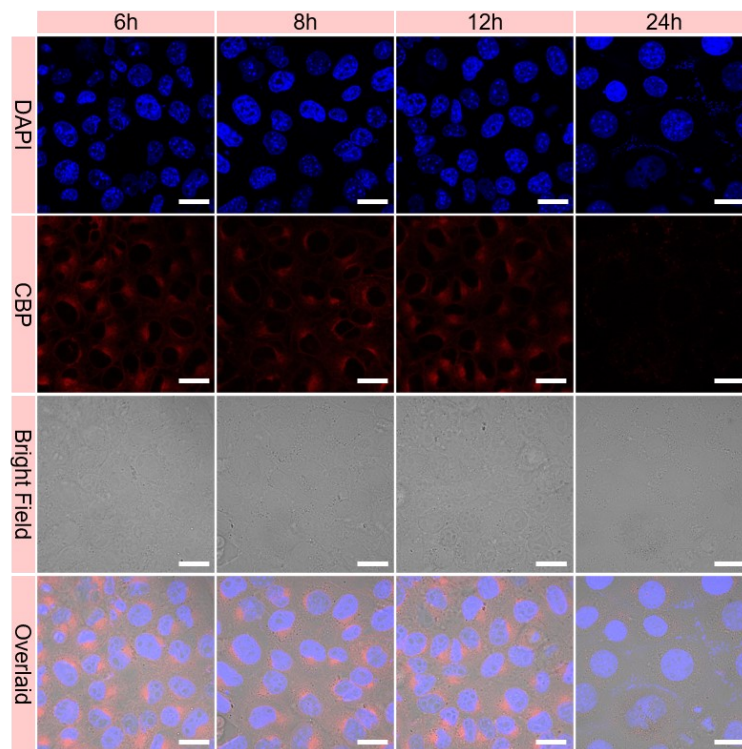


Fig. S6. Confocal fluorescence microscope images of cells co-incubated with CBP NPs at a different time from 6 to 24 h (Scale bar = 50 μ m).

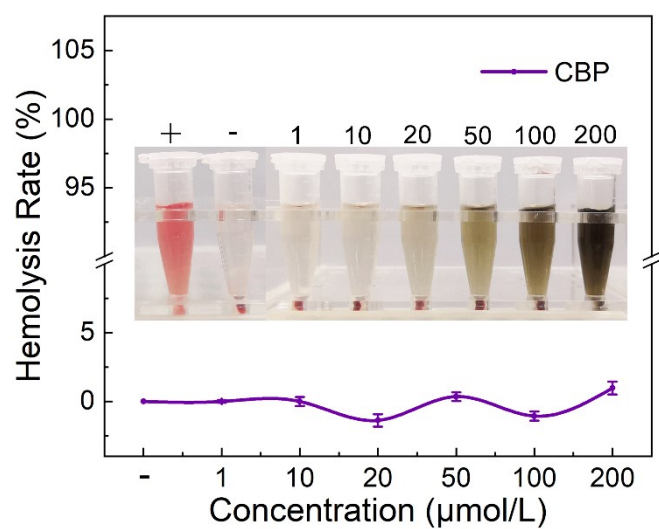


Fig. S7. Hemolysis rate of CBP NPs at different concentrations from 0 to 200 μM.

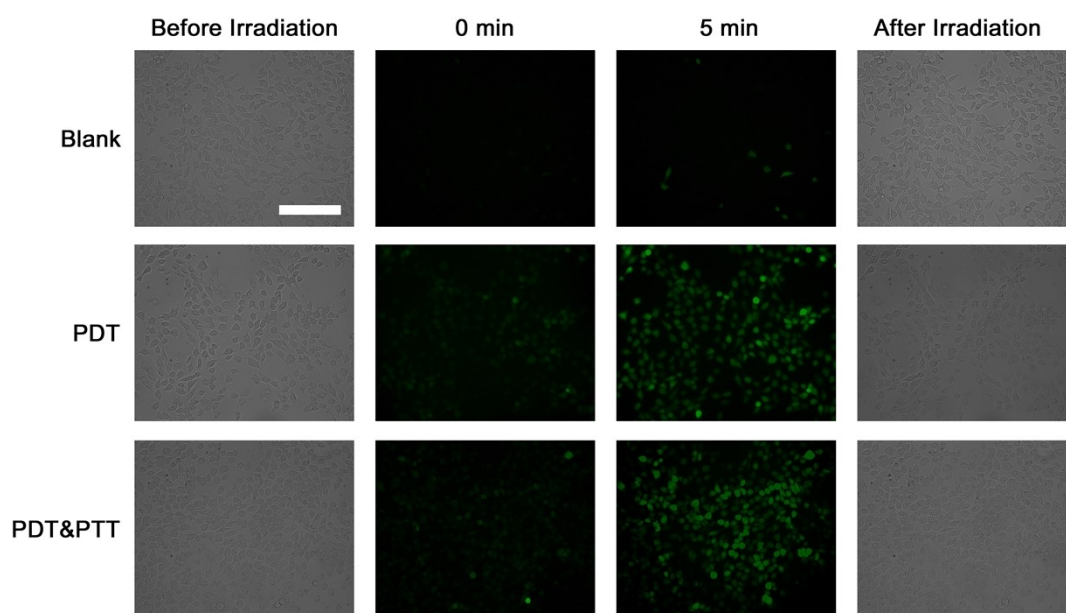


Fig. S8. Evaluation of intracellular ROS production before and after light irradiation.

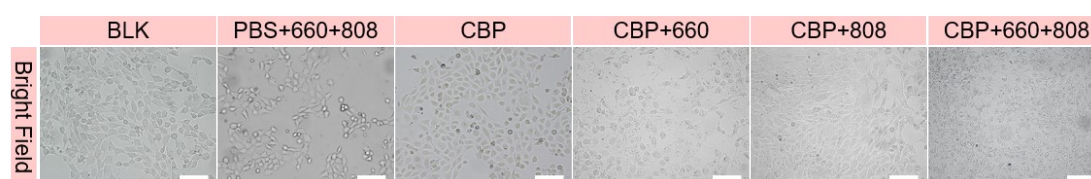


Fig. S9. Bright field photograph of live and dead staining of cells treated under different conditions (Scale bar = 200 μm).

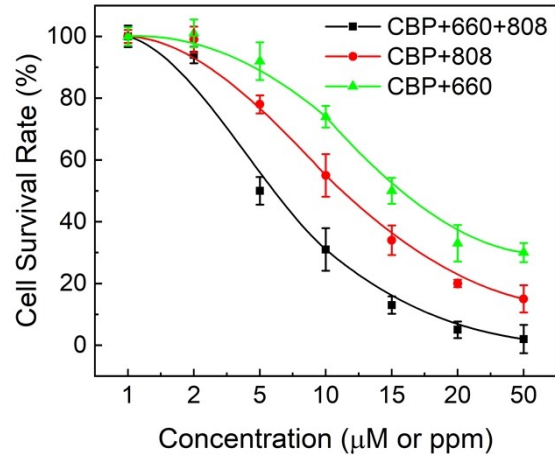


Fig. S10. The *in vitro* phototherapeutic effect of CBP NPs under different conditions. (μM is the concentration unit for Ce6 while ppm is the concentration unit for PDA)

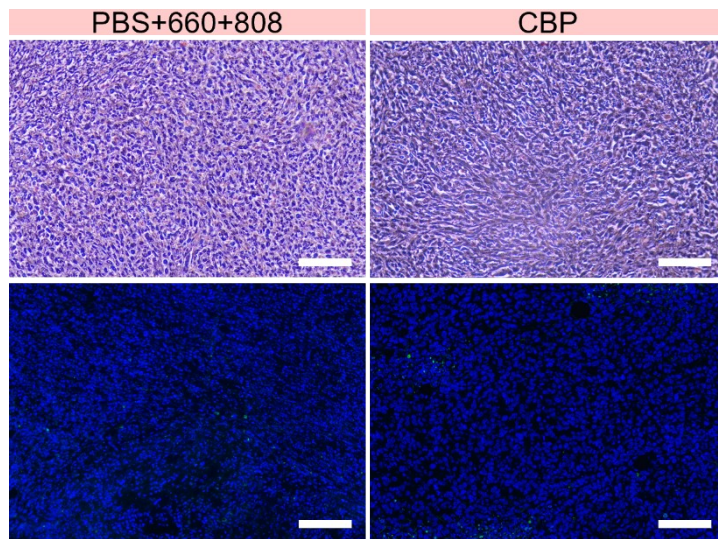


Fig.S11. Representative photographs of H&E and TUNEL staining imaging of the tumor sections of tumor-bearing mice of two groups (PBS combined with dual-mode laser irradiation and CBP NPs alone) (Scale bar is 200 μm).

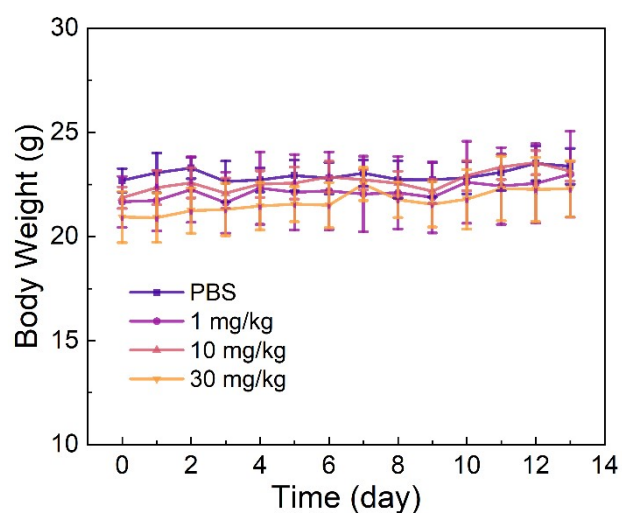


Fig. S12. Average body weight of four groups of mice injected PBS solution, CBP NPs suspensions with low, medium, and high concentrations, respectively. (n=5)

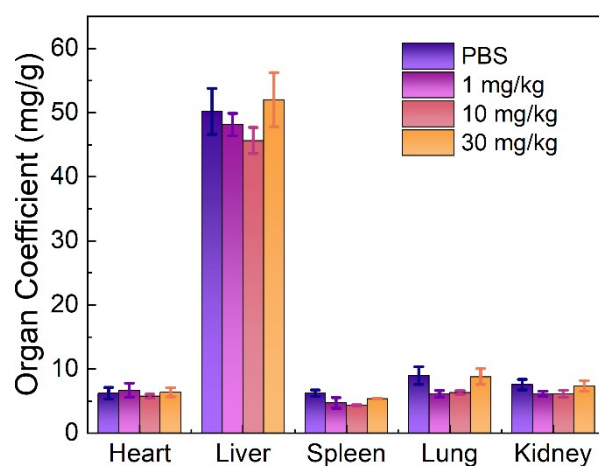


Fig. S13. Main organ coefficients of four groups of mice injected PBS solution, CBP NPs suspensions with low, medium, and high concentrations, respectively. (n=5)